Mathematical Modeling of VSB-Based Digital Television Systems

Hyoung-Nam Kim, Yong-Tae Lee, and Seung Won Kim

We mathematically analyze the passband vestigial sideband (VSB) system for the Advanced Television Systems Committee (ATSC) digital television standard and present a baseband-equivalent VSB model. The obtained baseband VSB model is represented by convolution of the transmission signal (before modulation) and the baseband equivalent of the complex VSB channel. Due to the operation of the physical channel as an RF passband and the asymmetrical property of VSB modulation, it is necessary to use a complex model. However, the passband channel may be reduced to an equivalent baseband. We show how to apply standard channel model information such as delay, gain, and phase for multiple signal paths to compute both the channel frequency response with a given carrier frequency and the resulting demodulated impulse response. Simulation results illustrate that the baseband VSB model is equivalent to the passband VSB model.

Manuscript received Jan. 9, 2002; revised May 16, 2002.

This work was supported in part by the Ministry of Information and Communication of Korea.

Hyoung-Nam Kim (phone: +82 42 860 5161, e-mail: kimhn@etri.re.kr), Yong-Tae Lee (e-mail: ytlee@etri.re.kr), and Seung Won Kim (e-mail: swkimm@etri.re.kr) are with DTV Transmission Research Team, ETRI, Daejeon, Korea.

I. INTRODUCTION

For the terrestrial digital television (DTV) standard of the Advanced Television Systems Committee (ATSC), the 8-vestigial sideband (VSB) has been adopted as a modulation method [1], [2]. Compared to the coded orthogonal frequency division multiplexing (COFDM) modulation of the European and Japanese DTV standard, the VSB transmission system has the advantage of a wide coverage area but suffers from multipath fading [3]. To solve the problem, there have been many efforts in various directions. One of the major approaches has been to develop an efficient equalization method [4].

Since VSB modulation has an asymmetrical property, a VSB-modulated signal includes quadrature components as well as in-phase ones. This means that the in-phase and quadrature components affect each other under multipath fading channels. Thus, to improve the performance of the VSB system, precise modeling is crucial. Since simulating a passband system is difficult and inefficient, it has been replaced with baseband-equivalent system simulation [5]. To simplify simulation, in [4] Ghosh did not consider modulation. However, in VSB-based systems, the modulation itself may critically affect received symbols. To raise the reliability of developed methods that use simulation, it is desirable to include modulation-associated effects.

In this paper, we mathematically analyze the 8-VSB system used for the ATSC standard and derive a baseband-equivalent VSB model. If channel information, such as delay, gain, and phase, is given, the derived model shows clearly the characteristics of the channel, since it reflects the VSB modulation effect on the equivalent channel. Thus, the equivalent model is efficiently used for baseband simulations to improve the performance of the VSB system, especially in the

equalization part. Furthermore, passband-related effects, such as a carrier frequency offset and phases of multiple echoes in DTV channels, are easily implemented in our model. This provides a reliable and efficient simulation model for enhancing sync/timing recovery and carrier recovery in the VSB system.

Applying channel information specified by the Advanced Television Technology Center (ATTC) [7] and the multipath profile used for the Brazil Laboratory test [8] to our mathematical channel model, we show how the given channels are represented in the form of the baseband-equivalent VSB channel model.

II. MODELING THE VSB-BASED SYSTEM

Figure 1 depicts a functional block diagram of the passband VSB system for the ATSC DTV standard [1], [2]. We first explain the role of each block and mathematically describe the passband VSB system model in sections II.1 through II.7. From the result of the mathematical description, we get the baseband-equivalent VSB system model revealed in section II.8.

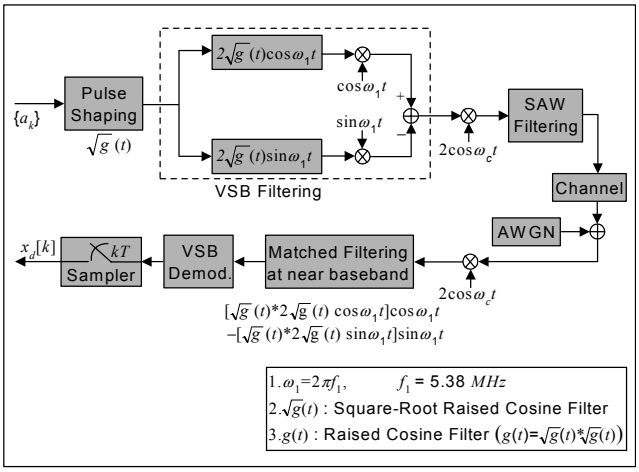

Fig. 1. Passband VSB system.

1. Pulse Shaping

Letting $\{a_k\}$ be an information symbol sequence and $s(t)$ a continuous-time signal comprised of the information symbols, we obtain

$$s(t)=\sum_{k=0}^{\infty} a_k \delta(t-kT), \tag{1}$$

where T is the symbol duration of 0.093 μs in the ATSC DTV standard in which the symbol rate is 10.76 MHz [1]. In order to avoid inter-symbol interference (ISI), a pulse-shaping filter (PSF) satisfying the Nyquist criterion is used at the transmitter [6]. For such a PSF, we use a raised-cosine (RC) filter comprised of a pair of square-root-raised-cosine (SRRC) filters, one at the transmitter and one at the receiver [1]. Note that the SRRC filter at the receiver is used for matched-filtering. Let $g(t)$ and $\sqrt{g}(t)$ denote the RC filter and the corresponding SRRC filter whose spectrum is shown in Fig. 2 [1]. These two functions have the relationship of

$$g(t)=\sqrt{g}(t)*\sqrt{g}(t), \tag{2}$$

where $*$ denotes a convolution operator. Note that for notational convenience, $\sqrt{g}(t)$ is used to represent the inverse Fourier transform (FT) of $\sqrt{G(f)}$ and is different from $\sqrt{g(t)}$. The pulse-shaped signal $x(t)$ is given by

$$x(t)=s(t)*\sqrt{g}(t)=\sum_{k=0}^{\infty} a_k \sqrt{g}(t-kT). \tag{3}$$

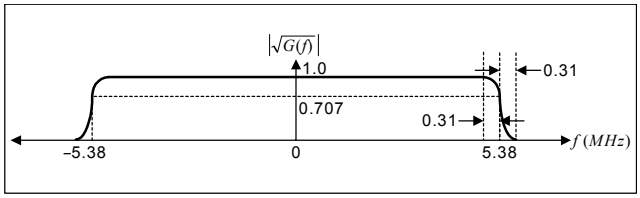

Fig. 2. Spectrum of a square-root-raised-cosine filter.

2. VSB Filtering and Up-Converting

The pulse-shaped signal is filtered by the VSB filter and then up-converted with the near-baseband frequency of 5.38 MHz corresponding to half of the symbol rate. Figure 3 shows the procedure for VSB filtering (Fig. 3(a)) and up-converting (Fig. 3(b)) in the frequency domain. The resulting complex signal $x_v(t)$ can be obtained as

$$x_v(t)=\underbrace{\overbrace{[x(t)*2\sqrt{g}(t)e^{j\omega_1 t}]}^{\text{VSB filtering}}e^{j\omega_1 t}}_{\text{Up-converting}}, \tag{4}$$

where $$\omega_1=2\pi f_1 \tag{5}$$

and $f_1=1/2T$ denotes the bandwidth of the VSB signal given by 5.38 MHz. Taking the real part of $x_v(t)$ produces the real signal (Fig. 3(c)) for transmission

$$\begin{aligned} x_{v,R}(t) &= \mathrm{Re}\{[x(t)*2\sqrt{g}(t)e^{j\omega_1 t}]e^{j\omega_1 t}\} \\ &= x_I(t)\cos\omega_1 t - x_Q(t)\sin\omega_1 t, \end{aligned} \tag{6}$$

where $$x_I(t)=x(t)*2\sqrt{g}(t)\cos\omega_1 t, \tag{7}$$

$$x_Q(t)=x(t)*2\sqrt{g}(t)\sin\omega_1 t. \tag{8}$$

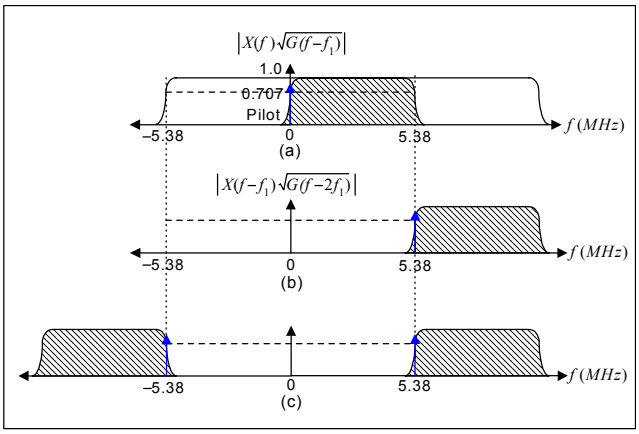

Fig. 3. VSB filtering and up-converting: (a) VSB filtering, (b) up-converting to the near-baseband frequency, and (c) extracting the real part for transmission.

3. Up-Converting to Passband and SAW Filtering

The VSB modulated signal is up-converted with a carrier frequency of ω_c by multiplying $e^{j\omega_c t}$. The complex passband signal now becomes

$$x_s(t) = x_v(t)e^{j\omega_c t} = \left(x_I(t) + jx_Q(t)\right) e^{j(\omega_c+\omega_1)t}. \quad (9)$$

Taking the real part of $x_s(t)$, we obtain the real passband signal for transmission given by

$$x_{s,R}(t) = x_I(t)\cos(\omega_c+\omega_1)t - x_Q(t)\sin(\omega_c+\omega_1)t. \quad (10)$$

Note that in a realistic implementation of the VSB transmitter, the real passband signal is obtained from $x_{v,R}(t)$ by multiplying $2\cos\omega_c t$. A SAW filter then extracts only the upper-sideband components of the up-converted signal. The process is shown in Fig. 4 and is described as follows:

$$\begin{aligned} x_{s,R}(t) &= F_{SAW}\left\{x_{v,R}(t)\times 2\cos\omega_c t\right\} \\ &= x_I(t)\cos(\omega_c+\omega_1)t - x_Q(t)\sin(\omega_c+\omega_1)t, \end{aligned} \quad (11)$$

where $F_{SAW}\{\cdot\}$ denotes a passband filtering with the SAW filter.

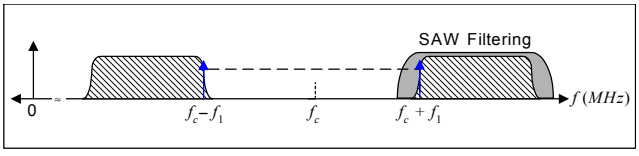

Fig. 4. Up-converting to passband and SAW filtering.

4. Multipath Fading Channel

Consider linear and time-invariant FIR channels. Multipath fading is the major cause of channel distortion. Three factors are usually considered for the multipath fading effect:

- α_i : attenuation constant at *i*-th path
- θ_i : phase shift at *i*-th path
- τ_i : relative time delay at *i*-th path

The output of the channel distorted by such effects is given by

$$\begin{aligned} x_c(t) &= \sum_{i=-N_1}^{N_2} \alpha_i x_I(t-\tau_i)\cos[(\omega_c+\omega_1)(t-\tau_i)+\theta_i] \\ &\quad - \sum_{i=-N_1}^{N_2} \alpha_i x_Q(t-\tau_i)\sin[(\omega_c+\omega_1)(t-\tau_i)+\theta_i] \\ &\quad + w(t) \\ &= \sum_{i=-N_1}^{N_2} \alpha_i\left[x_I(t-\tau_i)\cos\phi_i - x_Q(t-\tau_i)\sin\phi_i\right] \\ &\quad \times\cos(\omega_c+\omega_1)t \\ &\quad - \sum_{i=-N_1}^{N_2} \alpha_i\left[x_Q(t-\tau_i)\cos\phi_i + x_I(t-\tau_i)\sin\phi_i\right] \\ &\quad \times\sin(\omega_c+\omega_1)t \\ &\quad + w(t), \end{aligned} \quad (12)$$

where $$\phi_i = \theta_i - (\omega_c+\omega_1)\tau_i, \quad (13)$$

N_1 and N_2 are the numbers of the pre-cursors and post-cursors of the channel, respectively, and $w(t)$ is a white Gaussian noise process with a power spectral density of σ_w^2. From (12) and (13) we can see that since ϕ_i varies with ω_c, even in the same multipath conditions, the received signal is affected differently according to the carrier frequency.

Extension to time-varying channels can be easily obtained by changing the related parameters into the functions of time, such as $\alpha_i \to \alpha_i(t)$, $\tau_i \to \tau_i(t)$, and $\phi_i \to \phi_i(t)$. However, for notational convenience, we deal with time-invariant cases.

5. Down-Converting to Near-Baseband

At the receiver, the signal distorted by multipath fading of the channel is first down-converted to the near-baseband prior to matched filtering. Though the complex signal notations make the derivation of a baseband-equivalent channel clearer, we use real signal notations for considering realistic implementation of VSB-based DTV receivers. Let ε be the phase difference between the carrier frequency and the oscillator frequency of the synchronous detector. Using the oscillator, we obtain the near-baseband received signal $x_r(t)$ given by

$$
\begin{aligned}
x_r(t) &= x_c(t)\cdot 2\cos(\omega_c t-\varepsilon)\\
&= \sum_{i=-N_1}^{N_2}\alpha_i\cos(\phi_i+\varepsilon)\\
&\quad\times\underbrace{\left[x_I(t-\tau_i)\cos\omega_1 t - x_Q(t-\tau_i)\sin\omega_1 t\right]}_{x_{rI}(t)}\\
&\quad-\sum_{i=-N_1}^{N_2}\alpha_i\sin(\phi_i+\varepsilon)\\
&\quad\times\underbrace{\left[x_Q(t-\tau_i)\cos\omega_1 t + x_I(t-\tau_i)\sin\omega_1 t\right]}_{x_{rQ}(t)}\\
&\quad+w(t)\cdot 2\cos(\omega_c t-\varepsilon).
\end{aligned}
\tag{14}
$$

6. Matched Filtering

Under the white noise condition, matched filtering maximizes the signal-to-noise ratio (SNR) of the received signal [6]. We compute the output of the matched filter at near-baseband. The impulse response of the filter is given by

$$
\begin{aligned}
\sqrt{g}_M(t) &= \left(\sqrt{g}(t)*2\sqrt{g}(t)\cos\omega_1 t\right)\cos\omega_1 t\\
&\quad-\left(\sqrt{g}(t)*2\sqrt{g}(t)\sin\omega_1 t\right)\sin\omega_1 t.
\end{aligned}
\tag{15}
$$

Using (3) and (6), we show that the output of the matched filter $x_m(t)$ (the detailed computation is given in Appendix) becomes

$$
\begin{aligned}
x_m(t) &= x_r(t)*\sqrt{g}_M(t)\\
&= \sum_{i=-N_1}^{N_2}\alpha_i\cos(\phi_i+\varepsilon)\\
&\quad\times\{[s(t-\tau_i)*g_{MI}(t)]\cos\omega_1 t\\
&\quad-[s(t-\tau_i)*g_{MQ}(t)]\sin\omega_1 t\}\\
&\quad-\sum_{i=-N_1}^{N_2}\alpha_i\sin(\phi_i+\varepsilon)\\
&\quad\times\{[s(t-\tau_i)*g_{MQ}(t)]\cos\omega_1 t\\
&\quad+[s(t-\tau_i)*g_{MI}(t)]\sin\omega_1 t\}\\
&\quad+w(t)\cdot 2\cos(\omega_c t-\varepsilon)*\sqrt{g}_M(t),
\end{aligned}
\tag{16}
$$

where
$$g_{MI}(t) = g(t)*2g(t)\cos\omega_1 t, \tag{17}$$

$$g_{MQ}(t) = g(t)*2g(t)\sin\omega_1 t. \tag{18}$$

7. VSB Demodulation

We demodulate the matched filtered signal by down-converting to the baseband and low-pass filtering. The down-converted signal is obtained by multiplying the matched filtered signal by $2\cos\omega_1 t$ as follows:

$$
\begin{aligned}
&x_m(t)\cdot 2\cos\omega_1 t\\
&= \sum_{i=-N_1}^{N_2}\alpha_i\cos(\phi_i+\varepsilon)\\
&\quad\times\{[s(t-\tau_i)*\ g_{MI}(t)](1+\cos 2\omega_1 t\ )\\
&\quad+[s(t-\tau_i)*g_{MQ}(t)]\sin 2\omega_1 t\}\\
&\quad-\sum_{i=-N_1}^{N_2}\alpha_i\sin(\phi_i+\varepsilon)\\
&\quad\times\{[s(t-\tau_i)*g_{MQ}(t)](1+\cos 2\omega_1 t\ )\\
&\quad+[s(t-\tau_i)*g_{MI}(t)]\sin 2\omega_1 t\}\\
&\quad+w(t)\cdot 2\cos(\omega_c t-\varepsilon)\\
&\quad*\left[\left(\sqrt{g}(t)*2\sqrt{g}(t)\cos\omega_1 t\right)(1+\cos 2\omega_1 t\ )\right.\\
&\quad\left.-\left(\sqrt{g}(t)*2\sqrt{g}(t)\sin\omega_1 t\right)\sin 2\omega_1 t\right].
\end{aligned}
\tag{19}
$$

Low-pass filtering of the down-converted signal yields

$$
\begin{aligned}
x_d(t) &= F_{LOW}\{x_m(t)\cdot 2\cos\omega_1 t\}\\
&= \sum_{i=-N_1}^{N_2}\alpha_i\cos(\phi_i+\varepsilon)\cdot[s(t-\tau_i)*g_{MI}(t)]\\
&\quad-\sum_{i=-N_1}^{N_2}\alpha_i\sin(\phi_i+\varepsilon)\cdot[s(t-\tau_i)*g_{MQ}(t)]\\
&\quad+w(t)*\sqrt{g}(t)*2\sqrt{g}(t)\cos\omega_1 t,
\end{aligned}
\tag{20}
$$

where $F_{LOW}\{\cdot\}$ denotes a low pass filtering, and we used the approximation of

$$w(t)\cdot 2\cos(\omega_c t-\varepsilon)\approx w(t).$$

This approximation is reasonable because $w(t)$ is a white process.

8. Complete Baseband Model

From the demodulated signal $x_d(t)$ in (20), we can get a baseband-equivalent VSB channel model. Letting

$$\beta_i = \alpha_i\cos(\phi_i+\varepsilon)\quad\text{and}\quad\gamma_i = \alpha_i\sin(\phi_i+\varepsilon),$$

and using (17), (18), and the relationship of

$$s(t-\tau_i) = s(t)*\delta(t-\tau_i),$$

we obtain

$$
\begin{aligned}
x_d(t) &= \sum_{i=-N_1}^{N_2}[\beta_i h_I(t-\tau_i)-\gamma_i h_Q(t-\tau_i)]*g(t)*s(t)\\
&\quad+w(t)*\sqrt{g}(t)*2\sqrt{g}(t)\cos\omega_1 t,
\end{aligned}
\tag{21}
$$

where $\delta(t)$ is the Dirac-Delta function and

$$h_I(t) = 2g(t)\cos\omega_1 t, \tag{22}$$

$$h_Q(t) = 2g(t)\sin\omega_1 t. \tag{23}$$

Thus, we find the real impulse response of the baseband-equivalent VSB channel model $h_R(t)$ by rewriting (21) as

$$x_d(t) = h_R(t) * g(t) * s(t) + \sqrt{g}(t) * 2\sqrt{g}(t)\cos\omega_1 t * w(t), \tag{24}$$

where $$h_R(t) = \sum_{i=-N_1}^{N_2} [\beta_i h_I(t-\tau_i) - \gamma_i h_Q(t-\tau_i)]. \tag{25}$$

Consequently, the discrete-time equivalent channel is obtained by uniformly sampling $h_R(t)$ at an integer fraction of the symbol period T/M and is given by

$$h_R[n] = \sum_{i=-N_1}^{N_2} (\beta_i h_I[n-d_i] - \gamma_i h_Q[n-d_i]), \tag{26}$$

where $$n = \frac{kT}{M} \quad \text{and} \quad d_i = \left\lfloor \frac{M}{T}\tau_i + 0.5 \right\rfloor. \tag{27}$$

Note that k is a symbol index (refer to (1)) and $\lfloor \cdot \rfloor$ denotes a truncated integer.

Figure 5 shows the discrete-time baseband equivalent VSB system model simplified from Fig. 1 by mathematical modeling of the passband VSB system. All the filtering for the signal is included in the pulse shaping and VSB baseband equivalent channel, and therefore the effects of matched filtering and demodulation on the noise component are included in a separate block before the noise is added. Note that the noise is not subject to the channel model since it is physically generated at the receiver.

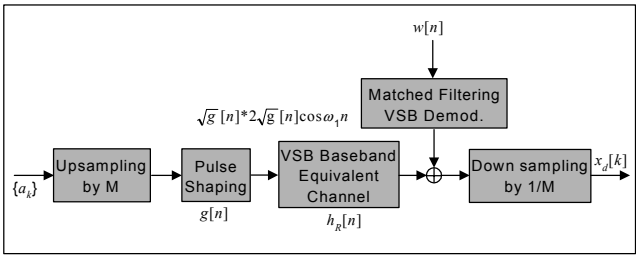

Fig. 5. Discrete-time baseband equivalent VSB system ($n = \frac{kT}{M}$).

III. SIMULATION RESULTS

We present simulation results corroborating the results of the derived VSB system model. First, the ideal channel is used for verifying our passband VSB modeling. Then, by introducing two well-known DTV channels, we illustrate that our derived baseband-equivalent VSB model is equivalent to the passband model.

1. Ideal Channel

To verify our mathematical derivation procedure, we first apply it to the ideal channel of the passband VSB system in Fig. 1. At each step the output is presented as the form of the impulse response. To achieve this, the information symbol sequence $\{a_k\}$ is set to be an impulse sequence.

The pulse-shaped signal $x(t)$ and its FT $X(f)$ is shown in Fig. 6. Note that this signal is identical to the pulse-shaping filter $\sqrt{g}(t)$ since $s(t)$ is the impulse signal. Figure 7 shows the impulse response and the frequency response of the VSB-filtered signal at the near-baseband frequency of f_1. In Fig. 8, the resulting signal after up-converting to passband and SAW filtering is shown. For convenience's sake, the carrier frequency f_c is set at $5f_1$ (26.9 MHz). Since the applied channel is ideal, the passband signal is down-converted to the near-baseband frequency at the receiver without being distorted by any channel effects. At this frequency band, matched filtering of the down-converted signal is carried out. The down-converted signal and the matched filtered signal are shown in Figs. 9 and 10, respectively. Finally, in order to do VSB demodulation, the matched-filtered signal is down-converted to baseband. Figure 11 shows that the demodulated signal is exactly equal to the impulse response of the raised-cosine filter for pulse shaping.

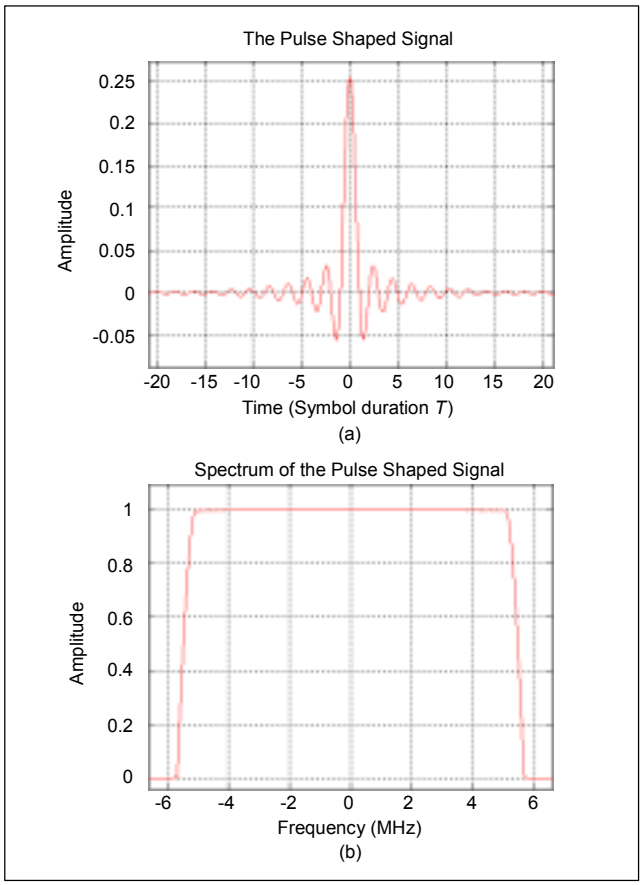

Fig. 6. The pulse-shaped signal: (a) impulse response, (b) frequency response.

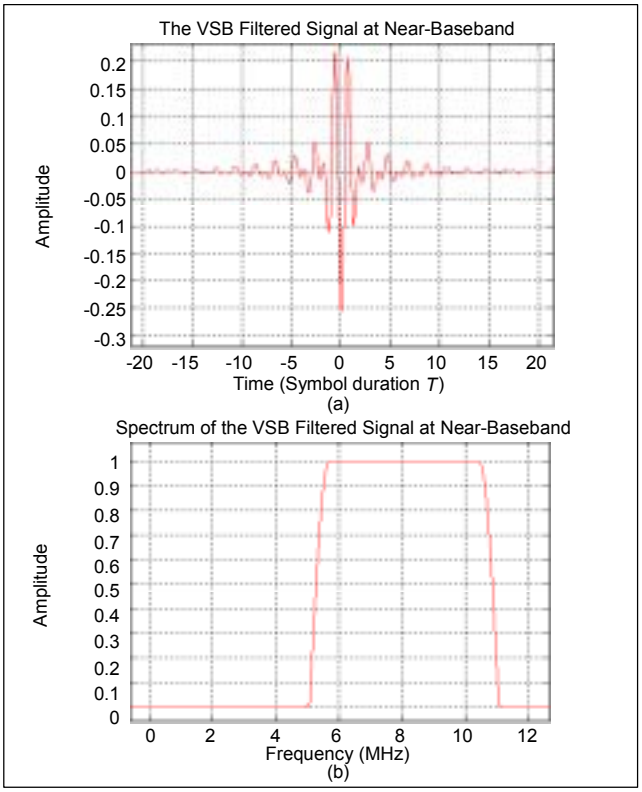

Fig. 7. The VSB-filtered signal: (a) impulse response, (b) frequency response.

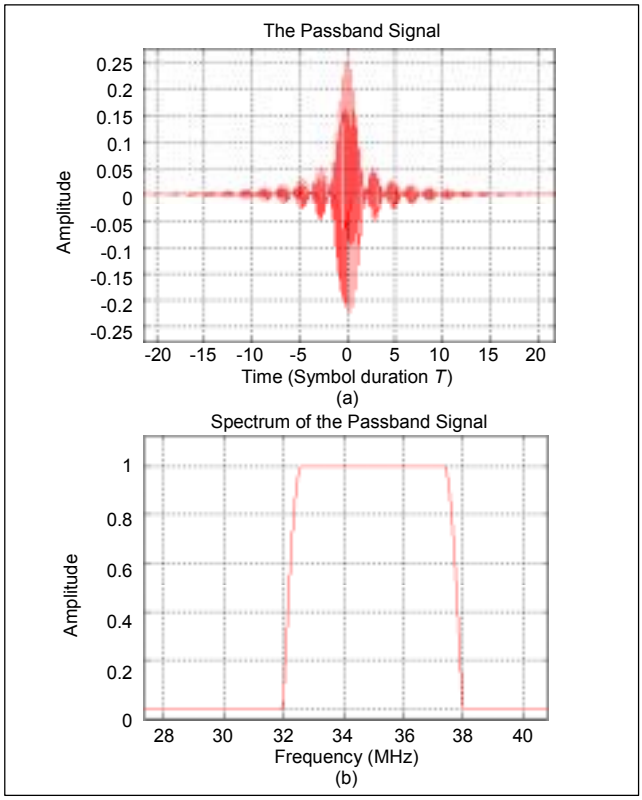

Fig. 8. The passband signal: (a) impulse response, (b) frequency response.

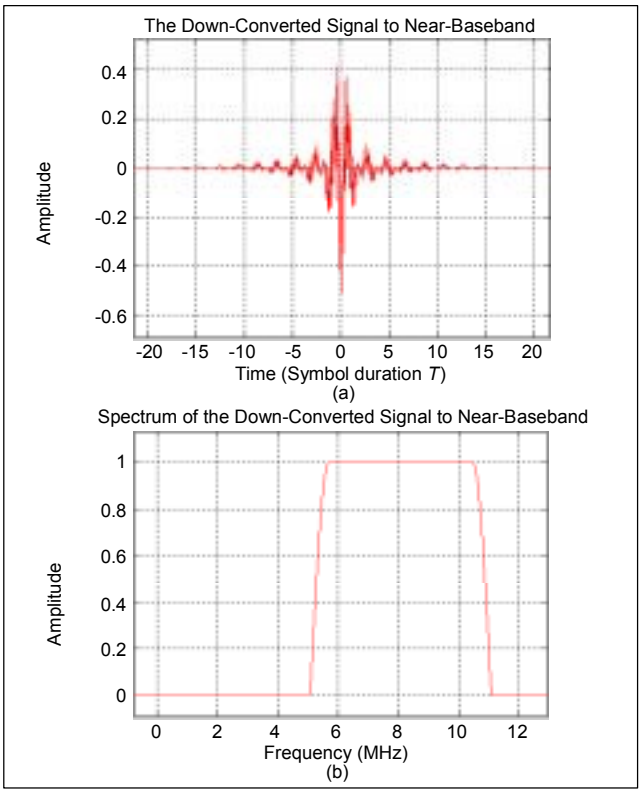

Fig. 9. The down-converted signal: (a) impulse response, (b) frequency response.

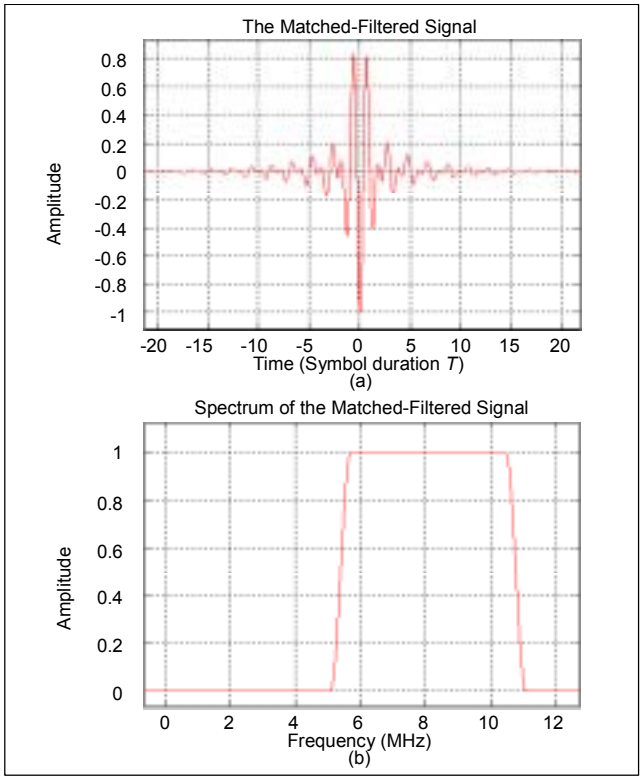

Fig. 10. The matched-filtered signal: (a) impulse response, (b) frequency response.

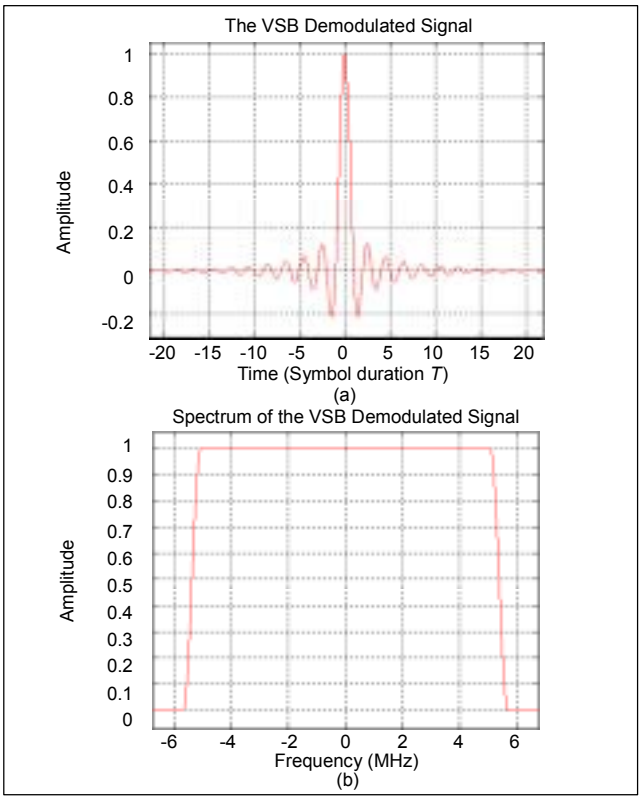

Fig. 11. The demodulated signal: (a) impulse response, (b) frequency response.

This verifies that our passband VSB system modeling is appropriate.

2. Channel Example I – ATTC Type B Channel

For the first example, we introduced channel information specified by the ATTC [7]. The channel is an ensemble of five echoes with delays, amplitudes, and phases, which are given in Table 1. The amplitude and frequency responses of the VSB channel combined with the pulse-shaping filter are shown in Figs. 12(a) and (b), respectively. The response of the passband modeling was obtained by feeding the impulse input into the pulse-shaping filter and then drawing the output of the sampler in the passband VSB system in Fig. 1. On the other hand, the response of the baseband modeling was the impulse response of the combined system of the pulse shaping filter and the baseband-equivalent channel ($g[n] * h_R[n]$). Figure 12 shows that the derived baseband-equivalent model is equal to the passband model of the VSB system. Though the difference between the two models is not clearly shown in Fig. 12, the maximum value of the difference was 3.9683×10^{-4}. The difference was caused simply by the numerical imprecision of calculation and was small enough to be ignored. Comparing the frequency response of the obtained VSB channel with that of the raised cosine filter in Fig. 12(b), we can see how severe the condition of the given channel in the VSB system is. Note that the frequency response of the raised cosine filter corresponds to the ideal channel.

Table 1. ATTC type B channel.

Delay (μs)	Amplitude (dB)	Phase (degree)
–1.75	–20	45
0.0	0	0
+0.197	–20	167
+1.80	–10	25
+5.75	–14	66
+17.95	–18	225

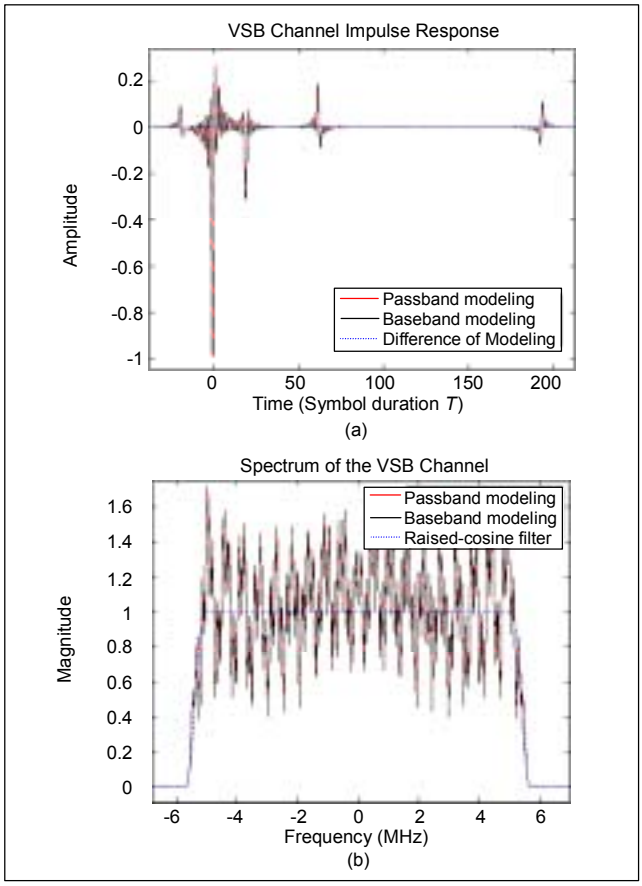

Fig. 12. ATTC B channel: (a) impulse response, (b) frequency response.

3. Channel Example II – Brazil Type D Channel

The second example is the Brazil type D channel, which modeled the indoor channel situation used for the Laboratory Test in Brazil [8]. The channel information is given in Table 2.

Unfortunately, this channel does not have phase information and thus the quadrature channel effect cannot be obtained. The amplitude and frequency responses of the VSB channel combined with the pulse-shaping filter are shown in Figs. 13(a) and (b), respectively. As in the previous example of the ATTC type B channel, Fig. 13 shows that the baseband-equivalent model is equal to the passband model of the VSB system. In this case, the maximum value of the difference was 4.6023×10^{-4}, which is caused simply by the numerical imprecision of the calculation. The figure clearly shows the characteristics of the given channel in the VSB-based system to compare the frequency response of the obtained VSB channel with that of the raised cosine filter in Fig. 13(b). Since this channel has more deep nulls than the ATTC type B channel, it is more difficult to equalize it than the ATTC type B channel.

Table 2. Brazil type D channel.

Delay (μs)	Amplitude (dB)
–5.71	–0.1
–5.23	–3.9
–3.64	–2.6
–2.81	–1.3
0.0	0
+0.07	–2.8

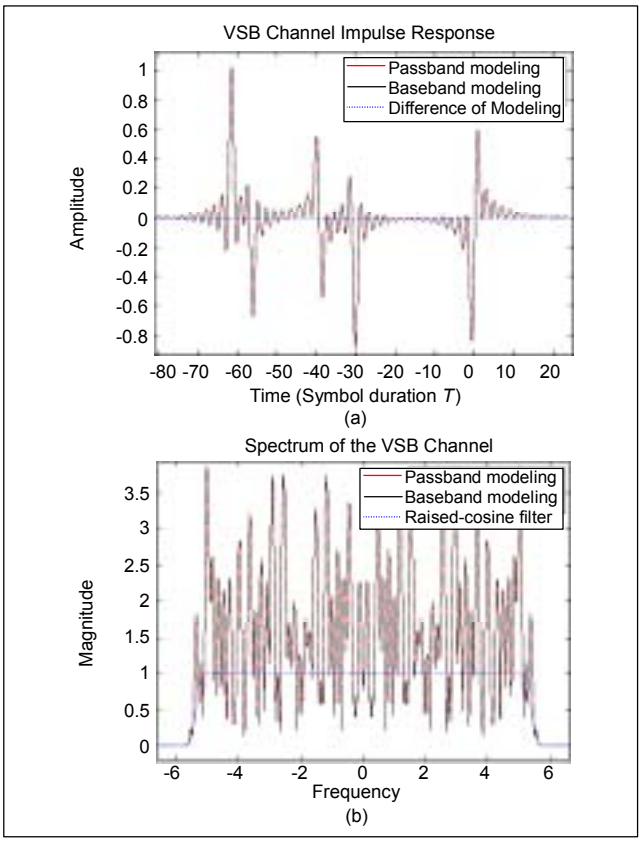

Fig. 13. Brazil D channel: (a) impulse response, (b) frequency response.

4. Application Examples of the Baseband-Equivalent VSB Channel

To show the usefulness of the derived baseband-equivalent VSB channel, we present two examples. One is the VSB channel under Korean DTV CH 14 for which the center frequency is 473 MHz. The other is the VSB channel under Korean DTV CH 15 for which the center frequency is 479 MHz. The same multipath profile of ATTC type B channel was applied to both cases. Figures 14 and 15 show the baseband-equivalent VSB channels obtained directly from $h_R[n]$ under Korean DTV CH 14 and CH 15, respectively. As noted in section II.4, we can see that even under the same multipath conditions, VSB channels differ according to carrier frequencies.

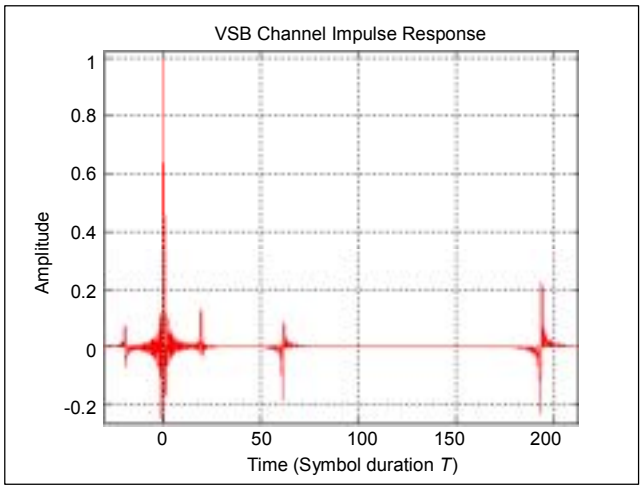

Fig. 14. ATTC B channel under Korean DTV CH 14.

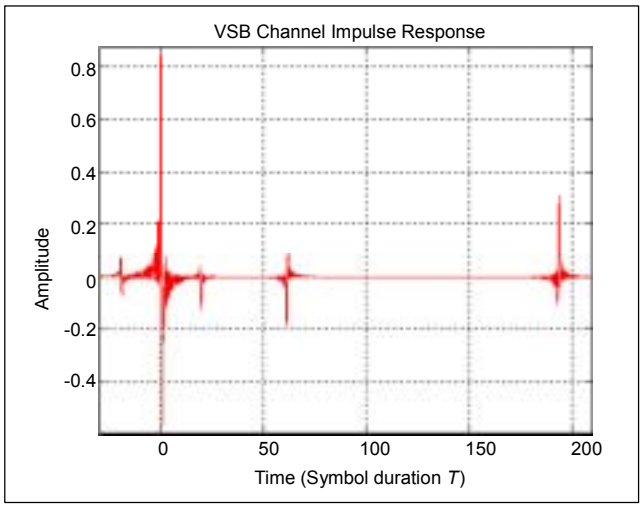

Fig. 15. ATTC B channel under Korean DTV CH 15.

Now suppose that we used the passband model instead of the baseband-equivalent model for this simulation. For 479 MHz, the sampling rate will not be smaller than 958 MHz, which increases tremendously the number of simulated samples. The increase of the sample number makes the simulation very inefficient and difficult due to the required time and memory allocation. To avoid such problems, using a sampling rate less than 958 MHz, for example, 26.9 MHz as in section III.1, results in an aliasing problem in RF band and thus the simulation results become unreliable.

IV. CONCLUSIONS

A baseband-equivalent VSB channel model has been derived by mathematically analyzing the VSB system for the ATSC DTV standard. Since VSB modulation has an asymmetric property, though channel information, such as delays, amplitudes, and phases, is given, the impulse response of the corresponding channel cannot be directly shown. In this paper, however, we show that with the derived model it can be easily obtained from such channel information. Therefore, the baseband-equivalent VSB model derived here shows the effects of modulation frequency as well as channel models in VSB-based systems, and thus it is very useful for simulations of the VSB system performed to improve its performance, especially in the equalization part.

ACKNOWLEDGEMENT

The authors would like to thank the anonymous reviewers whose comments improved this paper.

APPENDIX: COMPUTATION OF MATCHED FILTERING

The output of the matched filter is easily obtained in the frequency domain using the Fourier transform (FT). Letting $\sqrt{G}_M(f)$ be an FT of the matched filter $\sqrt{g}_M(t)$ in (15), we have

$$\begin{aligned}\sqrt{G}_M(f) &= \left[\sqrt{G(f)}\left(2\sqrt{G(f)} * \frac{\delta(f-f_1)+\delta(f+f_1)}{2}\right)\right] \\ &\quad * \frac{\delta(f-f_1)+\delta(f+f_1)}{2} \\ &\quad - \left[\sqrt{G(f)}\left(2\sqrt{G(f)} * \frac{\delta(f-f_1)-\delta(f+f_1)}{2j}\right)\right] \\ &\quad * \frac{\delta(f-f_1)-\delta(f+f_1)}{2j} \\ &= \sqrt{G(f-f_1)}\sqrt{G(f-2f_1)} \\ &\quad + \sqrt{G(f+f_1)}\sqrt{G(f+2f_1)}.\end{aligned} \tag{28}$$

Next, in order to get an FT of the input of the matched filter, $x_r(t)$, in (14), substituting (3), (7), and (8) into (14) yields

$$\begin{aligned}x_{rI}(t) &= [s(t-\tau_i) * \sqrt{g}(t) * 2\sqrt{g}(t)\cos\omega_1 t]\cos\omega_1 t \\ &\quad - [s(t-\tau_i) * \sqrt{g}(t) * 2\sqrt{g}(t)\sin\omega_1 t]\sin\omega_1 t\end{aligned} \tag{29}$$

and

$$\begin{aligned}x_{rQ}(t) &= [s(t-\tau_i) * \sqrt{g}(t) * 2\sqrt{g}(t)\sin\omega_1 t]\cos\omega_1 t \\ &\quad + [s(t-\tau_i) * \sqrt{g}(t) * 2\sqrt{g}(t)\cos\omega_1 t]\sin\omega_1 t.\end{aligned} \tag{30}$$

The FT of $x_{rI}(t)$ becomes

$$\begin{aligned}&X_{rI}(f) \\ &= S(f-f_1)e^{-j2\pi(f-f_1)\tau_i}\sqrt{G(f-f_1)}\sqrt{G(f-2f_1)} \\ &\quad - S(f+f_1)e^{-j2\pi(f+f_1)\tau_i}\sqrt{G(f+f_1)}\sqrt{G(f+2f_1)}\end{aligned} \tag{31}$$

and that of $x_{rQ}(t)$ becomes

$$\begin{aligned}&X_{rQ}(f) \\ &= \frac{1}{j}\Big(S(f-f_1)e^{-j2\pi(f-f_1)\tau_i}\sqrt{G(f-f_1)}\sqrt{G(f-2f_1)} \\ &\quad + S(f+f_1)e^{-j2\pi(f+f_1)\tau_i}\sqrt{G(f+f_1)}\sqrt{G(f+2f_1)}\Big),\end{aligned} \tag{32}$$

where $S(f)$ is the FT of $s(t)$. Applying (31) and (32) to (14), we obtain the FT of $x_r(t)$,

$$X_r(f) = \sum_{i=-N_1}^{N_2}\alpha_i\cos(\phi_i+\varepsilon)X_{rI}(f) - \sum_{i=-N_1}^{N_2}\alpha_i\sin(\phi_i+\varepsilon)X_{rQ}(f) \tag{33}$$

and then that of the output of the matched filter, $x_m(t)$,

$$\begin{aligned}X_m(f) &= X_r(f)\cdot\sqrt{G}_M(f) \\ &= \sum_{i=-N_1}^{N_2}\alpha_i\cos(\phi_i+\varepsilon) \\ &\quad \times\Big(S(f-f_1)e^{-j2\pi(f-f_1)\tau_i}G(f-f_1)G(f-2f_1) \\ &\quad - S(f+f_1)e^{-j2\pi(f+f_1)\tau_i}G(f+f_1)G(f+2f_1)\Big) \\ &\quad - \sum_{i=-N_1}^{N_2}\alpha_i\sin(\phi_i+\varepsilon) \\ &\quad \times\frac{1}{j}\Big(S(f-f_1)e^{-j2\pi(f-f_1)\tau_i}G(f-f_1)G(f-2f_1) \\ &\quad + S(f+f_1)e^{-j2\pi(f+f_1)\tau_i}G(f+f_1)G(f+2f_1)\Big) \\ &\quad + FT\{w(t)\cdot 2\cos(\omega_c t-\varepsilon)\}\cdot\sqrt{G}_M(f),\end{aligned} \tag{34}$$

where $FT\{\cdot\}$ denotes of a Fourier transform operator. Taking the inverse Fourier transform of $X_m(f)$ yields $x_m(t)$ as shown in (16).

REFERENCES

[1] Doc. A/53, *ATSC Digital Television Standard*, Sept. 1995.

[2] Doc. A/54, *Guide to the Use of ATSC Digital Television Standard*, Oct. 1995.

[3] Y. Wu, "Performance Comparison of ATSC 8-VSB and DVB-T COFDM Transmission Systems for Digital Television Terrestrial Broadcasting," *IEEE Trans. Consumer Electronics*, vol. 45, no. 3, Aug. 1999, pp. 916-924.

[4] M. Ghosh, "Blind Decision Feedback Equalization for Terrestrial Television Receivers," *Proc. of the IEEE*, vol. 86, no. 10, Oct. 1998, pp. 2070-2081.

[5] L.W. Couch, *Digital and Analog Communication Systems*, 6th ed., Prentice-Hall, 2001, pp. 240-245.

[6] J.G. Proakis, *Digital Communications*, 2nd ed., McGraw-Hill, New York, 1989.

[7] Comm. Research Center, "Digital Television Test Results – Phase I," *CRC Report No. CRC-RP-2000-11*, Ottawa, Nov. 2000, p. 6.

[8] Mackenzie, ABERT, and SET, "General Description of Laboratory Tests," *DTV Field Test Report in Brazil*, July 2000.

Hyoung-Nam Kim was born in Jeju, Korea, in 1970. He received the BS, MS, and PhD degrees in electronic and electrical engineering from Pohang University of Science and Technology (POSTECH), Pohang, in 1993, 1995, and 2000. Since 2000, he has been with the Broadcasting System Research Department, Electronics and Telecommunications Research Institute (ETRI), where he is a Senior Member of Research Staff. His research interests are in the area of digital signal processing, adaptive IIR filtering, and radar signal processing, in particular, signal processing for digital television, digital communications, and multimedia system. He is a member of IEEE and KICS.

Yong-Tae Lee was born in Daejeon, Korea on August 30, 1970. He received the BS, and MS degrees in avionics and electronic engineering from Hankuk Aviation University in 1993 and 1995. Since 1995, he has been with the Radio Signal Processing Department and Broadcasting System Research Department, Electronics and Telecommunications Research Institute (ETRI), where he is a Senior Member of Research Staff. His research interests are in the area of digital signal processing and RF signal processing, in particular, signal processing for digital television, digital communications and analog narrow band communications.

Seung Won Kim received his BSEE and MSEE from Sung Kyun Kwan University, Korea, in February 1986 and 1988. After graduation, he served in the Korea Army as a reserve officer from August 1988 to February 1989. Since June 1989, he has been employed at ETRI (Electronics and Telecommunications Research Institute), Korea. He received his PhD from University of Florida, USA, in May 1999. He is currently a Leader of the DTV Transmission Team at the ETRI. His main research interests are in the areas of digital communication systems, digital signal processing and DTV transmission systems.